Cerebellar contributions to biological motion perception in autism and typical development

Allison Jack[1,*], **Cara M. Keifer**[1], and **Kevin A. Pelphrey**[1]

[1]Yale University, Child Study Center, 230 South Frontage Rd., New Haven, CT, 06520, USA

Abstract

Growing evidence suggests that posterior cerebellar lobe contributes to social perception in healthy adults. However, we know little about how this process varies across age and with development. Using cross-sectional fMRI data, we examined cerebellar response to biological (BIO) versus scrambled (SCRAM) motion within typically developing (TD) and autism spectrum disorder (ASD) samples (age 4–30 y), characterizing cerebellar response and BIO > SCRAM-selective effective connectivity, as well as associations with age and social ability. TD individuals recruited regions throughout cerebellar posterior lobe during BIO > SCRAM, especially bilateral lobule VI, and demonstrated connectivity with right posterior superior temporal sulcus (RpSTS) in left VI, Crus I/II, and VIIIb. ASD individuals showed BIO > SCRAM activity in left VI and left Crus I/II, and bilateral connectivity with RpSTS in Crus I/II and VIIIb/IX. No between-group differences emerged in well-matched subsamples. Among TD individuals, older age predicted greater BIO > SCRAM response in left VIIb and left VIIIa/b, but reduced connectivity between RpSTS and widespread regions of the right cerebellum. In ASD, older age predicted greater response in left Crus I and bilateral Crus II, but decreased effective connectivity with RpSTS in bilateral Crus I/II. In ASD, increased BIO > SCRAM signal in left VI/Crus I and right Crus II, VIIb, and dentate predicted lower social symptomaticity; increased effective connectivity with RpSTS in right Crus I/II and bilateral VI and I-V predicted greater symptomaticity. These data suggest that posterior cerebellum contributes to the neurodevelopment of social perception in both basic and clinical populations.

Keywords

Cerebellum; Social Perception; Autistic Disorder; Magnetic Resonance Imaging; Human Development

Introduction

Theory regarding the etiology of autism spectrum disorder (ASD), a complex neurodevelopmental disorder, has often focused on functional deficits and histopathology in cerebral cortex [e.g., Geschwind and Levitt, 2007]. While cerebellar pathology is a well-

---

*Correspondence to Allison Jack, Ph.D., allison.jack@yale.edu.

Author Contributions
AJ and KP wrote the paper. AJ and CK conducted data analysis.

replicated finding in ASD that is receiving increasing attention, speculation about this structure's role in ASD often revolves around motor, language, or executive functioning deficits [Fatemi et al., 2012], rather than the social symptoms that many consider core to the disorder. This is likely due to the fact that the cerebellum's contributions to *typical* social function and development are not well understood.

Recent work indicates that in addition to participation in motoric, cognitive, and affective processes [Stoodley and Schmahmann, 2009], the cerebellum also contributes to social perception. In particular, regions of cerebellar posterior lobe (which includes portions of lobule VI as well as lobules Crus I, Crus II, and VIIb) participate during viewing of animate motion, whether this be point-light displays of human movement [Sokolov et al., 2010; Sokolov et al., 2012], hand motions [Jack et al., 2011], or more abstract displays of Heider and Simmel-type stimuli [Jack and Pelphrey, 2015]. A large activation likelihood estimation meta-analysis of cerebellar involvement in social cognition also indicated that viewing body part motion activates posterior lobe, with involvement of lobules VI, Crus I, and Crus II in particular [Van Overwalle et al., 2014]. However, there remain a number of open questions regarding cerebellar contributions to biological motion perception, particularly how this process varies across both typical and atypical development.

Developmental questions are particularly relevant with regards to the cerebellum in light of what we know about this structure's likely role in information processing. In particular, a better understanding of the cerebellum may help us to address one of the central questions of developmental neuroscience: what processes allow us to take complex skills and transform them from slow and effortful to rapid and efficient? A number of theorists [Bloedel, 1992; Ito, 1993; Ramnani, 2006; Schmahmann, 1996] have proposed that we use the cerebellum to make predictions about the cognitive consequences of cerebral activity, and that the experience-dependent refinement of these predictive models allows us to free up well-practiced functions from primarily top-down, effortful control. Further, they suggest that the cerebellum's widespread connectivity allows it to perform this function across a diverse array of information processing tasks. This framework suggests that the cerebellum could play an important role in development across multiple domains.

In the case of biological motion perception, regions of neocerebellum with connectivity to right posterior superior temporal sulcus (pSTS), a key cortical site for processing human movement [Allison et al., 2000], appear to play a role. Human imaging suggests an anatomical loop between pSTS and Crus I [Sokolov et al., 2014], and work in nonhuman primates appears to support this [Schmahmann and Pandya, 1991]. Moreover, during biological and animate motion perception, regions of cerebellar posterior lobe, particularly lobules Crus I, Crus II, and VIIb, demonstrate increased effective connectivity to pSTS [Jack et al., 2011; Jack and Pelphrey, 2015; and see also for meta-analysis Van Overwalle et al., 2015; Sokolov et al., 2012]. In line with these connectivity findings, analyses of local functional specialization indicate that a similar group of posterior cerebellar regions becomes selectively active while processing human or animate movements [Jack and Pelphrey, 2015; Sokolov et al., 2012].

While we are beginning to have evidence of how the posterior cerebellar lobe contributes to social perception in healthy adults, our understanding of how these contributions vary across development is poor. There is reason to suspect that the role of the posterior cerebellum, and its relationship with pSTS, may change with age; longitudinal morphometry indicates that the superior posterior lobe of the cerebellum has a more protracted developmental period than other regions of the cerebellum [Tiemeier et al., 2010], and that the peak developmental curve for the temporal lobe also occurs relatively late in adolescence [Giedd et al., 1999]. There is also reason to suspect that posterior cerebellar lobe has relevance in the neurodevelopment of social perception. In ASD, decreased grey matter is observed in right Crus I and left VIIIb across multiple studies [Stoodley, 2014] and lower grey matter volumes in right Crus I/II are associated with higher symptomaticity [D'Mello et al., 2015]. Further, among adolescents with the disorder, lower effective connectivity between right Crus I and pSTS during a social perception task is associated with greater difficulty reading the emotions and intentions of others [Jack and Morris, 2014]. Overall, while we have some understanding of how cerebellar shape and volume changes across development, both in typical and clinical populations, developmental studies of cerebellar *function*, especially in the domain of social perception, are extremely rare.

In this report, we address three main research aims: 1) to characterize the nature of cerebellar posterior lobe contributions to biological motion perception in both typically developing (TD) individuals and among individuals with a condition (ASD) often characterized by deficits in human motion perception; 2) to examine how these contributions vary by age; and 3) to assess whether variability in cerebellar posterior lobe activity and connectivity can predict social outcomes, particularly severity of social impairment in ASD. To address these aims, we describe the cerebellar response of TD and ASD individuals to passive viewing of coherent (BIO) versus scrambled (SCRAM) point-light displays of human motion, assessed via fMRI cross-sectionally. We predicted that, among TD individuals, cerebellar posterior lobe would be selectively active during perception of BIO > SCRAM, and would demonstrate effective connectivity with right pSTS (RpSTS); based on the notion that cerebellar processes reflect experience-dependent adaptation, we further predicted that posterior lobe activation and temporal connectivity would be positively associated with age. Additionally, we expected that if posterior cerebellar lobe indeed contributes meaningfully to the neurodevelopment of social perception, individual differences in this region's response should help explain variance in social behavior. Specifically, we predicted that response to biological motion in cerebellar posterior lobe, connectivity between this region and right pSTS, and associations between these patterns and age, would be attenuated in children with ASD. Further, we expected that higher levels of social atypicalities (assessed across both children with ASD and TD children) or of ASD-specific social symptoms (in children with ASD only) would be associated with lower involvement of posterior cerebellar lobe during biological motion perception.

Materials and Methods

Participants and sample selection

An in-house database was queried to identify fMRI scans obtained from TD and ASD participants using the biological motion paradigm. All datasets were originally acquired either from adults who had provided informed written consent, or from children whose parents had provided informed written consent and who had themselves provided written and/or verbal assent, as appropriate to their developmental level. If an adult with ASD was not his or her own legal guardian, his or her guardian (usually a parent) provided written informed consent and the participant provided verbal and written assent. Experimental procedures were all conducted in compliance with the standards established by the university Institutional Review Board and the Declaration of Helsinki. For all datasets, an accompanying high-resolution anatomical scan with low motion contamination was required. For child scans, an accompanying estimate of full scale IQ (Differential Abilities Scales [Elliott, 1990] or Wechsler Abbreviated Scale of Intelligence [Wechsler, 1999]) was required. For child ASD scans, accompanying diagnostic confirmation measures, the Autism Diagnostic Observational Schedule (ADOS) [Lord et al., 2000] and Autism Diagnostic Interview-Revised (ADI-R) [Lord et al., 1994] were required. For adult ASD scans, an ADOS and a full scale IQ estimate, but not an ADI-R, were required. The ADI-R, a parent interview, was not required for adults with ASD given the variability of parent involvement at that age and the greater difficulty of obtaining accurate retrospective information about early childhood milestones for adult subjects. All adult participants had diagnoses confirmed by ASD-expert clinicians at our center.

After screening, datasets were assessed for motion and cerebellar coverage. Exclusionary criteria included absolute or relative root mean squared (RMS) motion 3mm and/or 20% of timepoints identified as outliers [Power et al., 2012]. The extent of cerebellar functional coverage was consensus-coded (include/exclude) by two trained raters prior to analysis. See Figure 1A for a flow diagram detailing sample selection. Complete cerebellar coverage was rare; therefore, loss of a small portion of the most inferior regions (generally, inferior portions of lobules VIIIa/b and IX) was permitted. To achieve the best balance between group functional coverage and sample size, this set of preliminarily "accepted" functional images was registered into standard space (see below, "Cerebellar normalization") and, for each subject, the number of voxels lost in cerebellar grey matter was calculated relative to the standard cerebellar reference image. Subjects within the upper 15% of voxel loss for the entire group were then discarded from further analysis. A schematic of functional cerebellar coverage for the groups can be found in Figure 1B.

This sample selection process yielded 62 TD participants (26 male) ranging in age from 4.50 to 35.58 years and 35 participants (27 male) with ASD ranging in age from 7.08 to 30.08 years. Racial breakdown was as follows: for the TD sample, 39 participants identified as White, 9 as Black, 8 as Asian, 1 as native Hawaiian or other Pacific Islander, and 5 as more than one race; for the ASD sample, 29 participants identified as White, 3 as Black, 1 as Asian, and 2 as more than one race. Demographic information and data quality metrics for these samples are found in Table I. Several subsamples were generated from this group to

address a variety of research questions, with subsample creation driven either by availability of measure(s) of interest (e.g., a parent-report measure of social behavior not collected from adult participants), or the necessity of matching diagnostic groups on key nuisance variables prior to investigating group differences in brain activity. Subsample creation is described below ("Data analysis: Group-level fMRI statistics").

Experimental paradigm

Participants passively viewed blocks (6 per condition, 24 s each) of coherent point-light displays of biological motion (BIO) interleaved with scrambled (SCRAM) versions of these displays over a total of 144 two-second volumes, with an additional 10 volumes of final fixation. The displays were initially developed and described by Klin and colleagues [Klin et al., 2009] and the neural correlates of exposure to this paradigm at a whole-brain level, among both TD youth and youth with ASD, are well-understood [Kaiser et al., 2010]. The BIO > SCRAM contrast allows for assessment of brain activity associated with biological motion perception, controlling for visual motion perception generally [Bertenthal and Pinto, 1994].

Imaging parameters

Images were collected on a Siemens 3T Tim Trio scanner equipped with a 32-channel head-coil. Whole-brain T1-weighted anatomical images were acquired using a sagittal integrated parallel imaging sequence (TR = 2000 ms; TE = 2.96 ms; flip angle = 7°; FOV = 256 mm; image matrix 256 mm^2; voxel size = 1 mm^3; 160 slices; NEX = 1) or a magnetization-prepared rapid gradient-echo sequence (TR = 2530 ms; TE = 3.31 ms; flip angle = 7°; FOV = 256 mm; image matrix 256 mm^2; voxel size = 1 mm^3; 176 slices; NEX = 1). Whole-brain functional images were acquired using a single-shot, gradient-recalled echo planar pulse sequence (TR = 2000 ms; TE = 25 ms; flip angle = 60°; FOV = 220 mm; image matrix = 64 mm^2; voxel size = 3.4 mm × 3.4 mm × 4 mm; 34 slices) sensitive to blood oxygen level dependent contrast; 164 volumes were acquired, the first ten of which were discarded to allow for magnetic saturation effects.

Data analysis

FMRI preprocessing—FMRI data preprocessing was conducted using FSL's FEAT v. 6.00, and included motion correction [Jenkinson et al., 2002], slice-timing correction, skull-stripping [Smith, 2002], grand-mean intensity normalization of the entire 4D dataset by a single multiplicative factor, and highpass temporal filtering (Gaussian-weighted least-squares straight line fitting, with sigma = 50.0s). To prevent occipital activity from being smoothed across the cerebellar boundary prior to cerebellar extraction, no spatial smoothing occurred at this stage.

Cerebellar normalization—Functional and structural data were isolated from the cerebellum and registered to a standard cerebellar template, the Spatially Unbiased Infratentorial Template (SUIT) v. 2.7 [Diedrichsen, 2006; Diedrichsen et al., 2009]). The following steps were applied to each participant's anatomical image: setting image origin to the anterior commissure; image cropping and cerebellar masking; manual correction of the cerebellar mask; and normalization of the cropped, masked anatomical into SUIT space

using a nonlinear deformation. The preprocessed functional image was registered into high-resolution anatomical space using FSL's FLIRT [Jenkinson et al., 2002], and thereafter into SUIT space using the deformation matrix found during anatomical normalization. Functional images in SUIT space were then spatially smoothed [Smith and Brady, 1997] with a Gaussian kernel of FWHM 5mm, and submitted to first level statistical processing[1].

Single-subject fMRI statistics—At first level, data was submitted to fixed-effects analyses to generate subject-specific estimates of 1) cerebellar response to the BIO > SCRAM contrast, using a standard time-series modeling approach, and 2) BIO > SCRAM-specific connectivity to right pSTS, using a psychophysiological interaction (PPI) modeling approach. Both types of analyses were conducted using FSL's FEAT, with time-series statistical analysis carried out using FILM with local autocorrelation correction [Woolrich et al., 2001].

<u>**Time-series modeling of BIO > SCRAM:**</u> The timecourses of the BIO and SCRAM conditions were included as regressors in this analysis, convolved with a double-gamma hemodynamic response function (HRF). Temporal filtering was applied and a temporal derivative added. Nuisance regressors at this level were included to account for subject motion: a confound matrix identifying outlier timepoints according to the DVARS metric [Power et al., 2012] as well as six standard motion parameters. The contrast of interest from this analysis was the mean estimate of BIO > SCRAM.

<u>**PPI modeling:**</u> We used PPI analysis to examine task-related connectivity between the cerebellum and right pSTS, using the methods described in O'Reilly et al. [2012]. To create a seed region for this analysis, we conducted whole-brain analyses of the BIO > SCRAM contrast ($z > 2.3$, $p = 0.05$, cluster-corrected) separately for the full TD and ASD samples. To ensure that the seed would be inclusive of regions active across subsamples comprised wholly of children, whole-brain analyses were also conducted within a matched sample of TD children and children with ASD (Table I:C, see description of sample C in *Group-level fMRI analyses*, below). Results of the whole brain analyses are presented in the Supplementary Materials: Fig. S1 & Table SI. A binarized mask was created that represented overlap in whole-brain activity among: the full ASD sample, the full TD sample, children with ASD from the matched child sample, and TD children from the matched child sample. This mask was searched for coherent clusters in right pSTS; such a cluster of functional overlap was observed specifically in the posterior continuing (or posterior caudal [Segal and Petrides, 2012]) branch of the right STS. This portion of pSTS is often found to be selectively active during human motion perception [Pelphrey et al., 2003b; Pelphrey et al., 2005]. This right pSTS cluster was selected for use as a PPI seed (see Fig. 2G). The seed consisted of 107 voxels, with a center of gravity at x = 52.0, y = −55.5, z = 4.8 in MNI coordinates (mm). The anterior and posterior limits of the seed were y = −50 to −62; the superior and inferior limits were z = 8 to 2; and its lateral extent was between x = 60 and 42. A full description and schematics of the seed creation process can be found in Fig. S2. The

[1]A description of this approach, and scripts used to conduct it, are freely available at https://github.com/allisonjack/Cerebellum (CC BY-NC-SA 3.0 US)

seed mask was registered to individual functional space using FLIRT, and masks were visually inspected to ensure that no voxels encompassed non-brain material.

The first level analysis was modeled as follows: the psychological regressor was the timecourse of the BIO > SCRAM contrast, convolved with a double-gamma HRF and with temporal filtering applied and temporal derivative added. The physiological regressor was the mean time series from the right pSTS seed in functional space. The PPI regressor was the interaction term between the psychological and physiological regressors, with the psychological regressor zero-centered about the minimum and maximum values and the physiological regressor de-meaned. A regressor of no interest (BIO + SCRAM) was included to account for shared variance between trial types; it was convolved with a double-gamma HRF with temporal filtering applied and temporal derivative added. All convolutions were applied prior to forming the interaction term. Nuisance regressors representing standard motion parameters and motion outliers were also included at this level. The contrast of interest from this analysis was the mean estimate of the PPI regressor.

Group-level fMRI statistics—Group-level mixed-effects analyses were conducted on either the BIO > SCRAM contrast of parameter estimates (COPE; e.g., the statistical image containing the weighted β-values) images or on the COPE images that represented the PPI between the BIO > SCRAM contrast and the right pSTS timecourse (hereafter abbreviated BIO > SCRAM × RpSTS). All analyses were carried out using FSL's FLAME stages 1+2 with automatic outlier detection and deweighting [Beckmann et al., 2003; Woolrich et al., 2004; Woolrich, 2008], with cluster-corrected thresholding (using traditional Gaussian Random Field theory [Worsley, 2001]) at $z > 2.3$ and $p = .05$. Reporting of results is restricted to supra-threshold effects that could be assigned to any of the cerebellar lobules or nuclei with at least 25% confidence according to the probabilistic SUIT atlas [Diedrichsen et al., 2009]. To control for variability in functional data coverage, all group-level analyses included 4D voxelwise nuisance regressors representing regions of functional data loss for each individual. Pre-threshold masking was applied to limit investigation to cerebellar regions above z = −57 (in MNI coordinates) to minimize contamination of results due to EPI distortion. See Figure 1B for the cerebellar area analyzed, overlaid with a representation of voxelwise missingness. In all analyses, group variances were estimated separately.

We first examined average cerebellar response to BIO > SCRAM (or to BIO > SCRAM × RpSTS) and associations between cerebellar response and age. For both the full TD ($n = 62$) and full ASD ($n = 35$) groups (Table I:A, hereafter referred to as "sample A"), we created models that included two regressors of interest (in addition to the voxelwise nuisance regressor), one representing the group mean response, and the other representing age (centered). The contrasts of interest from these analyses were average group activation as well as positive or negative associations with age.

Given that these groups demonstrated mean differences in several important demographic and data quality assurance variables, we created matched subsamples for use in examining differences in brain activity between the TD and ASD groups. These matched samples were created using the R package "MatchIt" [Ho et al., 2007], with matches made to adult or child ASD cases from adult or child TD cases, respectively, based on average relative RMS

motion, maximum relative RMS motion, and sex. The resulting subsample characteristics, showing improved group balance, are reported in Table I. The matched sample that included both adults and children (Table I:B, "sample B", $N = 70$, TD & ASD group $n = 35$) was used to examine group differences in response to BIO > SCRAM (or to BIO > SCRAM × RpSTS), controlling for age; and to examine whether any group differences existed in the magnitude and/or direction of the association between age and cerebellar response to BIO > SCRAM.

To address our aim of understanding associations between autism-related social atypicalities and cerebellar response to biological motion, we incorporated information from parent-report measures of current and historical social function into our models. The Social Responsiveness Scale (SRS) is a measure designed to assess the presence of autistic features in the domains of social motivation, social communication, social awareness, social cognition, and restricted interests and repetitive behavior, among children ages 4 to 18 [Constantino and Gruber, 2005]. These features are assessed via parent agreement with a variety of statements on a 5-point Likert scale, and continuous scores are generated such that higher scores indicate endorsement of more responses consistent with social impairment. The SRS total t-score was of interest to us as a measure of current social impairment that was available for both TD children and children with ASD in our dataset. Thus, we tested the relationship between SRS total t-score and response to BIO > SCRAM (or to BIO > SCRAM × RpSTS) in motion-matched children (Table I:C, "sample C", $N = 54$, TD & ASD group $n = 27$). Two TD children did not have an SRS assessment available, and for these individuals scores were imputed by using the mean SRS total t-score for the TD group. SRS total t-score was not associated with age in this sample, $r = .12$, $p = .383$. Models using the matched child sample included regressors representing the mean BIO > SCRAM group response (or the mean BIO > SCRAM × RpSTS group response), age (grand-mean centered), FSIQ (grand-mean centered), and SRS total t-score (grand-mean centered). Positive and negative associations between SRS and BIO > SCRAM (or BIO > SCRAM × RpSTS) were assessed for each diagnostic group, as were interactions between diagnosis and SRS associations.

The ADI-R provided us with detailed information about historical functioning of individuals with ASD. Diagnostic algorithm A from this measure, "Qualitative Abnormalities in Reciprocal Social Interaction," is largely calculated based on parent responses regarding social abnormalities in their children between 4–5 years, but includes a few items based on the point of most severe symptom expression or a more developmentally relevant timepoint. Higher scores on this algorithm indicate that the individual has historically had a more severe symptom presentation in the social domain. In our sample, there was a moderate correlation between ADI-R:A scores and SRS total t-scores ($t(25) = .44$, $p = .022$). The ADI-R was available for $n = 30$ individuals with ASD (Table I:D, "sample D"). Models using this sample included regressors representing the mean BIO > SCRAM group response (or the mean BIO > SCRAM × RpSTS response), age (centered), FSIQ (centered), and ADI-R:A (centered). Positive and negative associations between ADI-R:A and BIO > SCRAM (or BIO > SCRAM × RpSTS) were assessed.

Post-hoc exploratory analyses—Upon conducting our planned analyses, we found indications that ipsilateral connectivity (i.e., between the right pSTS seed and right cerebellar hemisphere), versus the expected contralateral pattern, might be associated with younger age among TD individuals, and with greater social symptom load among individuals with ASD (see Results below). To further assess these patterns, we created a pSTS seed in the left hemisphere (LpSTS) that was the mirror image of the right pSTS seed used in the planned analyses, and ran the PPI models again using this left pSTS seed (BIO > SCRAM × LpSTS).

Results

Response to biological motion (TD)

TD individuals within the full sample (sample A, $n = 62$) displayed significant activity in response to BIO > SCRAM, controlling for age, in lobule VI bilaterally, with additional clusters bilaterally in VIIb/Crus II, VIIIa, and Crus I/II, as well as in vermis IX/VIIIb, left dentate nucleus, and left X (Fig. 2A; Table II). These individuals also demonstrated a significant BIO > SCRAM × RpSTS interaction in left lobules Crus I/II, VI, and VIIIb, as well as right lobules X and VIIIb (Fig. 2D; Table II). Post-hoc analysis of the BIO > SCRAM × LpSTS interaction revealed a largely similar set of regions to those found with the right hemisphere seed, comprising left lobules Crus I/II and VIIIa/b, and right lobules I-IV, VIIIa/b, and X (Fig. S3A; Table S2).

Response to biological motion (ASD)

ASD individuals within the full sample (sample A, $n = 35$) displayed a significant BIO > SCRAM response, controlling for age, within left lobules VI, Crus I, and Crus II (Fig. 2B; Table II). These individuals also demonstrated a significant BIO > SCRAM × RpSTS interaction in left Crus II and right hemispheric lobules Crus I/II, VIIIb, and IX (Fig 2E; Table II). Post-hoc analysis indicated that these participants also demonstrated a significant BIO > SCRAM × LpSTS interaction primarily limited to left Crus II (Fig. S3B; Table S2).

Group differences in response to biological motion

The mean BIO > SCRAM response of the full TD and ASD samples demonstrated overlap that occurred primarily in left VI, with some additional overlap in left Crus I/II (Fig. 2C). No significant group differences in BIO > SCRAM response, controlling for age, were detected in the matched sample that included both adults and children (sample B, $N = 70$). The full TD and ASD samples showed some overlap in the cerebellar regions that demonstrated a significant BIO > SCRAM × RpSTS interaction, primarily within left Crus II; however, no regions demonstrated significant between-group differences. Post-hoc analysis of the BIO > SCRAM × LpSTS interaction similarly showed no significant group difference.

Relationship between age and response to biological motion (TD)

Within the full sample of TD individuals (sample A), we observed a positive association between age and BIO > SCRAM response in left lobules VIIIa and VIIIb (Fig. 3A; Table III). There were no cerebellar regions that demonstrated a negative association between age and BIO > SCRAM response. By contrast, these individuals demonstrated a negative

association between BIO > SCRAM × RpSTS connectivity and age in regions of right lobules VIIb, VIIIa/b, VI, and Crus I/II, as well as left lobules I-IV (Fig. 3B; Table III), with the strongest association detected in right VI. No cerebellar regions demonstrated a positive association between age and BIO > SCRAM × RpSTS connectivity. Post-hoc analysis did not reveal any regions that demonstrated significant positive or negative associations between BIO > SCRAM × LpSTS connectivity and age in the full TD sample.

Relationship between age and response to biological motion (ASD)

Within the full sample of individuals with ASD (sample A), we observed positive associations between age and BIO > SCRAM response in left Crus I, left dentate nucleus, and left IX, as well as in right Crus II (Fig. 3A; Table III). No cerebellar regions demonstrated a negative association between age and BIO > SCRAM response. Conversely, no cerebellar regions demonstrated a positive association between age and BIO > SCRAM × RpSTS connectivity, but negative associations were observed bilaterally in Crus I/II (Fig. 3C; Table III). Post-hoc analysis indicated that participants with ASD also showed negative associations between age and BIO > SCRAM × LpSTS connectivity in bilateral Crus I/II, as well as in right VI, right IX, and vermis VIIIb (Fig. 6A; Table III).

Interactions between diagnostic status and the relationship between age and response to biological motion

We found no cerebellar regions displaying a group difference in the relationship between age and response to biological motion in our matched sample of adults and children (sample B), nor were any such differences found in the post-hoc BIO > SCRAM × LpSTS PPI analysis.

Current social impairment and response to biological motion (TD & ASD)

Among youth with ASD (sample C), lower parent-reported social impairment (as measured via SRS total *t*-score, and controlling for age and FSIQ) was related to greater BIO > SCRAM activity in right dentate nucleus (Fig. 4A; Table IV); no such associations were observed in the matched group of TD children. Among TD children, higher SRS scores were associated with stronger BIO > SCRAM × RpSTS connectivity in a cluster with a peak in right X, while among children with ASD, clusters demonstrating this pattern were observed in right hemispheric lobules Crus I and Crus II with extension into VIIb (Fig. 4B; Table IV). Post-hoc analysis did not reveal any regions that demonstrated significant positive or negative associations between BIO > SCRAM × LpSTS connectivity and SRS scores for either group.

Historical social functioning in ASD and response to biological motion

Lower parent-reported ASD symptoms in the social domain (measured via the ADI-R:A) were associated with higher BIO > SCRAM activity in left Crus I and right Crus II among individuals with ASD (sample D), controlling for age and FSIQ (Fig. 5A; Table V). Conversely, higher BIO > SCRAM × RpSTS connectivity was associated with greater symptom load in a cluster that encompassed regions of right Crus I, left VI, left V, and right VI, with extension into bilateral I-IV (Fig. 5B; Table V). Post-hoc analysis indicated that higher BIO > SCRAM × LpSTS connectivity was associated with greater symptom load in

left Crus I as well as in a primarily anterior lobe cluster that encompassed regions of left V, left VI and right I-IV (Fig. 6B; Table V).

Discussion

This report makes several contributions to the burgeoning literature on cerebellar contributions to nonmotor function, specifically in the relatively understudied area of social perception. Using datasets acquired during passive viewing of coherent versus scrambled point-light displays of human motion, we examined cerebellar response to these stimuli among both neurotypical participants and among individuals (those with ASD) known to exhibit deficits in social perception and behavior. Our aims were: 1) to characterize the topography of biological-motion-selective cerebellar response and temporo-cerebellar effective connectivity; 2), to examine associations between these responses and age; and 3), to examine associations between these responses and measures of social behavior. Overall, our findings reveal that 1) typically developing individuals recruit regions throughout cerebellar posterior lobe while viewing biological motion, especially lobule VI; moreover, they also demonstrate task-specific connectivity between posterior cerebellar lobe and right pSTS. Individuals with ASD also show posterior lobe activation and connectivity selective to this task, demonstrating overlap with TD response in left-hemispheric regions of VI and Crus I/II. 2) Among typically developing individuals, older age predicted greater cerebellar response in left VIIb and left VIIIa/b, but reduced effective connectivity between right pSTS and widespread regions of the right cerebellar hemisphere. Among individuals with ASD, older age predicted greater response in left Crus I and in Crus II bilaterally, and decreased effective connectivity with both left and right pSTS in bilateral Crus I/II. 3) Cerebellar response and connectivity predicted social symptom load among individuals with ASD in a number of regions. Specifically, increased signal in regions of left VI/Crus I and right Crus II, VIIb, and dentate nucleus was associated with ratings of less severe social impairment, and increased effective connectivity with right pSTS within right Crus I/II, more medial regions of left VI, and lobules I-V, was associated with greater social impairment. Post-hoc analysis indicated that increased effective connectivity with left pSTS within left Crus I was also associated with greater social impairment, suggesting that atypical lateralization of connectivity may be related to impairment. Associations between social behavior and cerebellar response among TD children were not widespread. Finally, contrary to our hypotheses, although analyses of our full TD and ASD samples displayed patterns of response and connectivity that appeared somewhat different topographically, we did not find statistically significant group differences in subsamples that were well-matched for head motion and age. Below, we further unpack these main findings.

TD individuals demonstrated a robust, well-formed response to coherent versus scrambled human motion across cerebellar posterior lobe, with the most prominent activity located in bilateral VI, and additional bilateral foci in Crus I, Crus II, VIIb, and VIIIa. Individuals with ASD showed activation in left VI and left Crus I/II. Although the topography of the cerebellar response to BIO > SCRAM among participants with ASD appeared somewhat different from that of our TD group, contrary to our hypothesis, we detected no regions in which there was a statistically significant difference in response within our matched sample of participants with ASD and TD participants. A previous study using point-light biological

motion stimuli to assess cerebellar response in healthy adults noted activation in left Crus I and VIIb [Sokolov et al., 2012]; the peak activity we observed in TD individuals was somewhat anterior, in lobule VI, although in both cases left VIIb is noted. Discrepancies between the topography of activation could be attributable to several factors. First, Sokolov and colleagues complemented the viewing of their stimuli with a one-back repetition task, while ours was passive; the difference in task requirements could help to explain the difference in response topography. Further, we used a larger sample ($N = 62$ versus $N = 13$) and analyzed the cerebellum in isolation, versus conducting a whole-brain analysis. This, combined with our use of the SUIT toolbox for more accurate registration of the individual cerebellar lobules [Diedrichsen, 2006], may have increased our statistical power. Inclusion of a broader age range may also have impacted the localization of the response.

The activation observed in VIIIa among our TD participants may seem counterintuitive, given reports that have characterized this site as primarily associated with sensorimotor processes [Stoodley and Schmahmann, 2009]. However, we have previously observed this region to be active in healthy adults when viewing abstract shapes whose motion patterns appear animate [Jack and Pelphrey, 2015], suggesting that it may play a role in social perception. Moreover, functional connectivity analysis indicates that the activity of lobule VIIIa correlates with that of occipito-temporal and secondary sensory as well as premotor regions, but not to primary motor regions, suggesting a role in secondary sensorimotor and integrative processes [Kipping et al., 2013]. Continued study of the inferior cerebellar lobules, including VIII, is needed to help clarify its role. One limitation of our project is that scans were not originally acquired for the purpose of assessing cerebellar signal, requiring us to adjust for individual differences in functional data loss and other sources of noise in inferior cerebellum via statistical methods. Ideally, however, scans would be acquired at outset to be optimized for signal capture from inferior cerebellum, including oblique slice prescription and acquisition of a field map to help correct for EPI distortions.

As predicted, TD participants showed significant human-motion-selective effective connectivity between right pSTS and left VI, left Crus I/II, and bilateral regions of VIIIb. Participants with ASD showed effective connectivity with right pSTS that was bilateral in Crus I/II and broader in spatial extent, with additional clusters showing this pattern of connectivity in bilateral IX. Previously, effective connectivity with pSTS selective to human or animate motion has been demonstrated in healthy adults in Crus I, Crus II, and VIIb [Jack et al., 2011; Jack and Pelphrey, 2015; Sokolov et al., 2012], and our results are in line with these previous findings.

Older age was associated with stronger response to the BIO > SCRAM contrast in left hemispheric VIIb, VIIIa, and VIIIb among TD individuals. Regions displaying this pattern in ASD were more superior, with positive associations between age and response to biological motion found in left Crus I and bilateral Crus II. Conversely, effective connectivity with right pSTS was reduced with age in a number of regions for both groups. In our TD sample, regions that showed this pattern were distributed throughout the right cerebellar hemisphere, suggesting that ipsilateral connectivity may decrease with age. Structurally, cerebro-cerebellar connections are largely crossed [Apps and Watson, 2013]; functions that are lateralized within the cerebrum tend to show a contralateral pattern of

representation in the cerebellar hemispheres [Jansen et al., 2005; Schlerf et al., 2015], with damage to left cerebellum disrupting right-lateralized cerebral cognitive functions (e.g., spatial processing) and vice versa [Scott et al., 2001]. Social perceptual functions of pSTS tend to be right-lateralized [e.g., Pelphrey et al., 2003a; Pelphrey et al., 2004], and the seed we chose *a priori* for PPI analysis was consequently in right pSTS. For these reasons, connectivity with the left cerebellar hemisphere would be expected, and indeed we find that on average, among TD participants, effective connectivity with right pSTS was predominantly observed in left cerebellum. It appears, however, that the degree to which this functional asymmetry is observed may differ with age. When the development of functional asymmetry within the cerebrum has been investigated, researchers have observed that the lateralization of both left- (e.g., linguistic) and right- (e.g., spatial) hemispheric functions may increase with age [Everts et al., 2009; Szaflarski et al., 2006]. However, while some aspects of cerebral lateralization may be related strictly to maturational processes [Stephan et al., 2007], it also appears likely that skill acquisition plays a key role in the development of functional asymmetry, particularly for more complex functions [Everts et al., 2009; Holland et al., 2007; Plante et al., 2015; Weiss-Croft and Baldeweg, 2015]. It is possible that the negative association between age and ipsilateral connectivity we observe could be related to similar processes, with an increasingly selective response over development either related to maturation or to accumulating experience with the stimuli. Given that afferent connectivity influences the development of lateralization in target regions [Stephan et al., 2007], the pattern we observe in right cerebellum may also be related to changes in pSTS response with age, such as decreasing recruitment of the left hemisphere. We note, however, that our post-hoc analysis of BIO > SCRAM × LpSTS did not reveal significant associations with age anywhere in cerebellum for our TD sample. Further, given that this investigation was cross-sectional, we lack the ability to draw links between individual experience and changes in cerebellar response. To clarify these processes in future, we must implement longitudinal designs that test both short-term development of cerebellar signal in response to repeated exposures to social stimuli, and long-term development of cerebellar function across childhood and adolescence.

Among children with ASD, stronger activation of clusters with peaks in left Crus I (with extension into left VI) and right Crus II during biological motion perception was associated with parent report of less severe social impairment historically according to diagnostic algorithm A of the ADI-R; greater activity in right dentate nucleus was associated with lower endorsement of current symptomaticity on the SRS. The association between left Crus I/VI response to biological motion and intact social perception aligns well with a number of previous findings. Lesions to this region have been associated with impaired biological motion detection [Sokolov et al., 2010], and stronger recruitment of this site among healthy adults while viewing ambiguous animate stimuli is related to a greater tendency to attribute socio-emotional properties to those stimuli [Jack and Pelphrey, 2015]. The association between lower symptom severity according to the SRS and greater BIO > SCRAM response in dentate nucleus was unexpected. The region displaying this pattern lies specifically in the dorso-rostral region of the right dentate nucleus (DRDN; above z = −35 and anterior to y = −58; [Küper et al., 2011]). This is somewhat unexpected given that it is the ventral region of dentate nucleus that tends to be linked with cognitive process, while the dorsal region has

been associated with motor functions [Habas, 2010; Küper et al., 2011; Tellmann et al., 2015]. However, intriguingly, portions of the dentatorubrothalamic pathway seeded from this specific sub-region of dentate nucleus—right DRDN—have been found to exhibit lower white matter integrity in children with ASD than in neurotypical children [Jeong et al., 2012]. Further, higher white matter integrity in the pathway emerging from right DRDN predicted better daily living skills in these children [Jeong et al., 2012]. These previous findings, coupled with our findings in the functional domain, suggest that deficits in right DRDN and its efferents may help characterize the ASD neuroendophenotype and predict behavioral outcomes.

Greater effective connectivity between right pSTS and regions of right Crus I and right Crus II were associated with greater symptomaticity as reported on the SRS; greater effective connectivity between right pSTS and right Crus I, medial sectors of lobule VI bilaterally, and anterior lobe (lobules I-V), were associated with poorer parent report of social functioning on the ADI-R. Connectivity between right pSTS and anterior lobe, which is a predominantly sensorimotor region of the cerebellum [e.g., Stoodley et al., 2012], during biological motion perception would indeed be suggestive of an atypical neural pattern, one potentially associated with social deficit. However, associations between right pSTS effective connectivity in posterior lobe regions and higher symptom load were unexpected; for example, it is currently unclear why greater BIO > SCRAM response in right Crus II would be associated with better social function, but that greater effective connectivity between this region and right pSTS would be associated with poorer social function. One possible explanation of this finding may be related to the fact that crossed cerebro-cerebellar connectivity is more developmentally typical, with (as we discussed above) increasing lateralization associated with age and experience. Thus, ipsilateral connectivity may be an index of atypical neurodevelopment that also marks greater social deficit. We note that individuals with ASD have previously been documented to exhibit atypical patterns of brain structural and functional asymmetry, either exhibiting a more symmetrical pattern or an asymmetry reversed from the typical direction [e.g., Cardinale et al., 2013; Floris et al., 2013; Floris et al., 2016; Kleinhans et al., 2008; Lo et al., 2011]; moreover, this atypical asymmetry is often documented in the temporal region [e.g., Jung et al., 2016; Lange et al., 2010; Rojas et al., 2005; Stroganova et al., 2007]. Such asymmetries have previously been shown to correlate with phenotypic profiles in ASD, as where atypical lateralization in language-associated brain regions [Floris et al., 2016; De Fossé et al., 2004] or electrophysiological components [Schmidt et al., 2009] have been found to predict linguistic deficits. It is possible that a similar process is at work here. In our post-hoc PPI analysis, we observed that increased connectivity between left pSTS and left Crus I also predicted greater social symptom load on the ADI-R. This may lend some support to the interpretation that ipsilateral temporo-cerebellar connectivity is indicative of a neuropathological process. However, given that we did not predict this outcome a priori, future work should attempt to reproduce the result in a larger sample of individuals with ASD. If replicable, additional experiments should be implemented to determine under what conditions effective connectivity between right pSTS and cerebellar posterior lobe predicts positive versus negative social outcomes.

In sum, we find that cerebellar posterior lobe contributes to response to human motion, across ages and in both typical and ASD populations. Age differences in activation and connectivity related to biological motion perception indicate the need for further longitudinal work to clarify how cerebellar interactions with neocortex, particularly pSTS, develop with individual experience. Further, evidence suggesting that cerebellar response, particularly in Crus I/II, is related to the degree of social impairment in children with ASD, indicates that developmental studies of this region could not only contribute to our understanding of typical social information processing, but also of factors that contribute to risk for, or resilience to, perturbations in social development.

Supplementary Material

Refer to Web version on PubMed Central for supplementary material.

Acknowledgments

References

Allison T, Puce A, McCarthy G. Social perception from visual cues: Role of the STS region. Trends Cogn Sci. 2000; 4:267–278. [PubMed: 10859571]

Apps, R., Watson, TC. Cerebro-Cerebellar Connections. In: Manto, M.Gruol, D.Schmahmann, JD.Koibuchi, N., Rossi, F., editors. Handbook of the Cerebellum and Cerebellar Disorders. Dordrecht: Springer Netherlands; 2013. p. 1131-1153.

Beckmann CF, Jenkinson M, Smith SM. General multilevel linear modeling for group analysis in FMRI. Neuroimage. 2003; 20:1052–1063. [PubMed: 14568475]

Bertenthal BI, Pinto J. Global processing of biological motions. Psychol Sci. 1994; 5:221–224.

Bloedel JR. Functional heterogeneity with structural homogeneity: How does the cerebellum operate? Behav Brain Sci. 1992; 15:666–678.

Cardinale RC, Shih P, Fishman I, Ford LM, Müller R-A. Pervasive rightward asymmetry shifts of functional networks in autism spectrum disorder. JAMA psychiatry. 2013; 70:975–82. [PubMed: 23903586]

Constantino, JN., Gruber, CP. Social Responsiveness Scale. Los Angeles, CA: Western Psychological Services; 2005.

D'Mello AM, Crocetti D, Mostofsky SH, Stoodley CJ. Cerebellar gray matter and lobular volumes correlate with core autism symptoms. NeuroImage Clin. 2015; 7:631–9. [PubMed: 25844317]

Diedrichsen J. A spatially unbiased atlas template of the human cerebellum. Neuroimage. 2006; 33:127–38. [PubMed: 16904911]

Diedrichsen J, Balsters JH, Flavell J, Cussans E, Ramnani N. A probabilistic MR atlas of the human cerebellum. Neuroimage. 2009; 46:39–46. [PubMed: 19457380]

Diedrichsen J, Zotow E. Surface-Based Display of Volume-Averaged Cerebellar Imaging Data. PLoS One. 2015; 10:e0133402. [PubMed: 26230510]

Elliott, CD. DAS Introductory and Technical Handbook. San Antonio, TX: The Psychological Corporation; 1990.

Everts R, Lidzba K, Wilke M, Kiefer C, Mordasini M, Schroth G, Perrig W, Steinlin M. Strengthening of laterality of verbal and visuospatial functions during childhood and adolescence. Hum Brain Mapp. 2009; 30:473–83. [PubMed: 18219619]

Fatemi SH, Aldinger KA, Ashwood P, Bauman ML, Blaha CD, Blatt GJ, Chauhan A, Chauhan V, Dager SR, Dickson PE, Estes AM, Goldowitz D, Heck DH, Kemper TL, King BH, Martin LA,

Millen KJ, Mittleman G, Mosconi MW, Persico AM, Sweeney JA, Webb SJ, Welsh JP. Consensus paper: pathological role of the cerebellum in autism. Cerebellum. 2012; 11:777–807. [PubMed: 22370873]
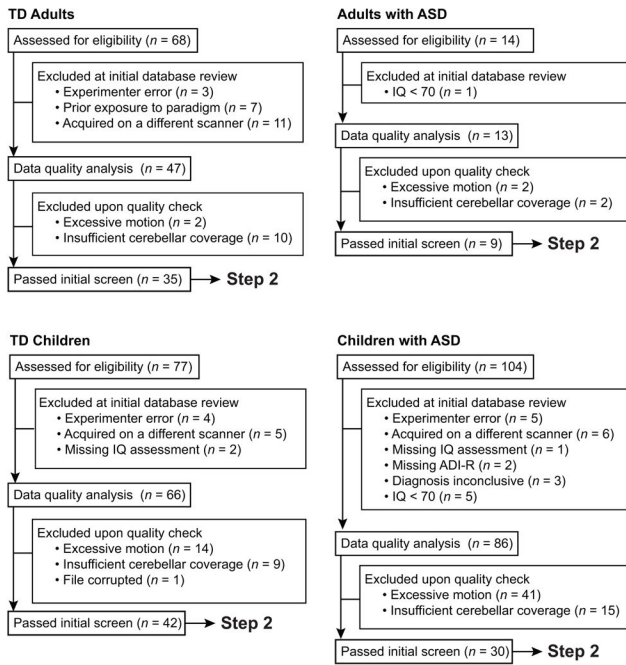
Floris DL, Chura LR, Holt RJ, Suckling J, Bullmore ET, Baron-Cohen S, Spencer MD. Psychological correlates of handedness and corpus callosum asymmetry in autism: the left hemisphere dysfunction theory revisited. J Autism Dev Disord. 2013; 43:1758–72. [PubMed: 23179344]

Floris DL, Lai M-C, Auer T, Lombardo MV, Ecker C, Chakrabarti B, Wheelwright SJ, Bullmore ET, Murphy DGM, Baron-Cohen S, Suckling J. Atypically rightward cerebral asymmetry in male adults with autism stratifies individuals with and without language delay. Hum Brain Mapp. 2016; 37:230–53. [PubMed: 26493275]

De Fossé L, Hodge SM, Makris N, Kennedy DN, Caviness VS, McGrath L, Steele S, Ziegler DA, Herbert MR, Frazier JA, Tager-Flusberg H, Harris GJ. Language-association cortex asymmetry in autism and specific language impairment. Ann Neurol. 2004; 56:757–66. [PubMed: 15478219]

Geschwind DH, Levitt P. Autism spectrum disorders: Developmental disconnection syndromes. Curr Opin Neurobio. 2007; 17:103–11.

Giedd JN, Blumenthal J, Jeffries NO, Castellanos FX, Liu H, Zijdenbos A, Paus T, Evans AC, Rapoport JL. Brain development during childhood and adolescence: a longitudinal MRI study. Nat Neurosci. 1999; 2:861–3. [PubMed: 10491603]

Habas C. Functional imaging of the deep cerebellar nuclei: a review. Cerebellum. 2010; 9:22–8. [PubMed: 19513801]

Ho DE, Imai K, King G, Stuart EA. Matching as Nonparametric Preprocessing for Reducing Model Dependence in Parametric Causal Inference. Polit Anal. 2007; 15:199–236.

Holland SK, Vannest J, Mecoli M, Jacola LM, Tillema J-M, Karunanayaka PR, Schmithorst VJ, Yuan W, Plante E, Byars AW. Functional MRI of language lateralization during development in children. Int J Audiol. 2007; 46:533–51. [PubMed: 17828669]

Ito M. Movement and thought: identical control mechanisms by the cerebellum. Trends Neurosci. 1993; 16:444–7. [PubMed: 7507614]

Jack A, Englander ZA, Morris JP. Subcortical contributions to effective connectivity in brain networks supporting imitation. Neuropsychologia. 2011; 49:3689–98. [PubMed: 21958651]

Jack A, Morris JP. Neocerebellar contributions to social perception in adolescents with autism spectrum disorder. Dev Cogn Neurosci. 2014; 10:77–92. [PubMed: 25170555]

Jack A, Pelphrey KA. Neural Correlates of Animacy Attribution Include Neocerebellum in Healthy Adults. Cereb Cortex. 2015; 25:4240–47. [PubMed: 24981794]

Jansen A, Flöel A, Van Randenborgh J, Konrad C, Rotte M, Förster A-F, Deppe M, Knecht S. Crossed cerebro-cerebellar language dominance. Hum Brain Mapp. 2005; 24:165–72. [PubMed: 15486988]

Jenkinson M, Bannister PR, Brady JM, Smith SM. Improved optimization for the robust and accurate linear registration and motion correction of brain images. Neuroimage. 2002; 17:825–41. [PubMed: 12377157]

Jeong J-W, Chugani DC, Behen ME, Tiwari VN, Chugani HT. Altered white matter structure of the dentatorubrothalamic pathway in children with autistic spectrum disorders. Cerebellum. 2012; 11:957–71. [PubMed: 22477362]

Jung CE, Strother L, Feil-Seifer DJ, Hutsler JJ. Atypical Asymmetry for Processing Human and Robot Faces in Autism Revealed by fNIRS. PLoS One. 2016; 11:e0158804. [PubMed: 27389017]

Kaiser MD, Hudac CM, Shultz S, Lee SM, Cheung C, Berken AM, Deen B, Pitskel NB, Sugrue DR, Voos AC, Saulnier CA, Ventola P, Wolf JM, Klin A, Vander Wyk BC, Pelphrey KA. Neural signatures of autism. Proc Natl Acad Sci USA. 2010; 107:21223–8. [PubMed: 21078973]

Kipping JA, Grodd W, Kumar V, Taubert M, Villringer A, Margulies DS. Overlapping and parallel cerebello-cerebral networks contributing to sensorimotor control: an intrinsic functional connectivity study. Neuroimage. 2013; 83:837–48. [PubMed: 23872155]

Kleinhans NM, Müller R-A, Cohen DN, Courchesne E. Atypical functional lateralization of language in autism spectrum disorders. Brain Res. 2008; 1221:115–25. [PubMed: 18555209]

Klin A, Lin DJ, Gorrindo P, Ramsay G, Jones W. Two-year-olds with autism orient to non-social contingencies rather than biological motion. Nature. 2009; 459:257–61. [PubMed: 19329996]

Küper M, Dimitrova A, Thürling M, Maderwald S, Roths J, Elles HG, Gizewski ER, Ladd ME, Diedrichsen J, Timmann D. Evidence for a motor and a non-motor domain in the human dentate nucleus--an fMRI study. Neuroimage. 2011; 54:2612–22. [PubMed: 21081171]

Lange N, Dubray MB, Lee JE, Froimowitz MP, Froehlich A, Adluru N, Wright B, Ravichandran C, Fletcher PT, Bigler ED, Alexander AL, Lainhart JE. Atypical diffusion tensor hemispheric asymmetry in autism. Autism Res. 2010; 3:350–8. [PubMed: 21182212]

Lo Y-C, Soong W-T, Gau SS-F, Wu Y-Y, Lai M-C, Yeh F-C, Chiang W-Y, Kuo L-W, Jaw F-S, Tseng W-YI. The loss of asymmetry and reduced interhemispheric connectivity in adolescents with autism: a study using diffusion spectrum imaging tractography. Psychiatry Res. 2011; 192:60–6. [PubMed: 21377337]

Lord C, Risi S, Lambrecht L, Cook EH, Leventhal BL, DiLavore PC, Pickles A, Rutter M. The Autism Diagnostic Observation Schedule-Generic: A standard measure of social and communication deficits associated with the spectrum of autism. J Autism Dev Disord. 2000; 30:205–23. [PubMed: 11055457]

Lord C, Rutter M, Le Couteur A. Autism Diagnostic Interview-Revised: a revised version of a diagnostic interview for caregivers of individuals with possible pervasive developmental disorders. J Autism Dev Disord. 1994; 24:659–85. [PubMed: 7814313]

O'Reilly JX, Woolrich MW, Behrens TEJ, Smith SM, Johansen-Berg H. Tools of the trade: psychophysiological interactions and functional connectivity. Soc Cogn Affect Neurosci. 2012; 7:604–9. [PubMed: 22569188]

Van Overwalle F, Baetens K, Mariën P, Vandekerckhove M. Social cognition and the cerebellum: a meta-analysis of over 350 fMRI studies. Neuroimage. 2014; 86:554–72. [PubMed: 24076206]

Van Overwalle F, D'aes T, Mariën P. Social cognition and the cerebellum: A meta-analytic connectivity analysis. Hum Brain Mapp. 2015; 36:5137–54. [PubMed: 26419890]

Pelphrey KA, Mitchell TV, McKeown MJ, Goldstein J, Allison T, McCarthy G. Brain activity evoked by the perception of human walking: Controlling for meaningful coherent motion. J Neurosci. 2003a; 23:6819–25. [PubMed: 12890776]

Pelphrey KA, Morris JP, Michelich CR, Allison T, McCarthy G. Functional anatomy of biological motion perception in posterior temporal cortex: An fMRI study of eye, mouth and hand movements. Cereb Cortex. 2005; 15:1866–76. [PubMed: 15746001]

Pelphrey KA, Singerman JD, Allison T, McCarthy G. Brain activation evoked by perception of gaze shifts: The influence of context. Neuropsychologia. 2003b; 41:156–70. [PubMed: 12459214]

Pelphrey KA, Viola RJ, McCarthy G. When strangers pass: Processing of mutual and averted social gaze in the superior temporal sulcus. Psychol Sci. 2004; 15:598–603. [PubMed: 15327630]

Plante E, Almryde K, Patterson DK, Vance CJ, Asbjørnsen AE. Language lateralization shifts with learning by adults. Laterality. 2015; 20:306–25. [PubMed: 25285756]

Power JD, Barnes KA, Snyder AZ, Schlaggar BL, Petersen SE. Spurious but systematic correlations in functional connectivity MRI networks arise from subject motion. Neuroimage. 2012; 59:2142–54. [PubMed: 22019881]

Ramnani N. The primate cortico-cerebellar system: anatomy and function. Nat Rev Neurosci. 2006; 7:511–22. [PubMed: 16791141]

Rojas DC, Camou SL, Reite ML, Rogers SJ. Planum temporale volume in children and adolescents with autism. J Autism Dev Disord. 2005; 35:479–86. [PubMed: 16134033]

Schlerf JE, Galea JM, Spampinato D, Celnik PA. Laterality Differences in Cerebellar-Motor Cortex Connectivity. Cereb Cortex. 2015; 25:1827–34. [PubMed: 24436320]

Schmahmann JD. From movement to thought: Anatomic substrates of the cerebellar contribution to cognitive processing. Hum Brain Mapp. 1996; 4:174–198. http://www.ncbi.nlm.nih.gov/pubmed/20408197. [PubMed: 20408197]

Schmahmann JD, Pandya DN. Projections to the basis pontis from the superior temporal sulcus and superior temporal region in the rhesus monkey. J Comp Neurol. 1991; 308:224–48. [PubMed: 1716269]

Schmidt GL, Rey MM, Oram Cardy JE, Roberts TPL. Absence of M100 source asymmetry in autism associated with language functioning. Neuroreport. 2009; 20:1037–41. [PubMed: 19491710]

Scott RB, Stoodley CJ, Anslow P, Paul C, Stein JF, Sugden EM, Mitchell CD. Lateralized cognitive deficits in children following cerebellar lesions. Dev Med Child Neurol. 2001; 43:685–91. [PubMed: 11665825]

Segal E, Petrides M. The morphology and variability of the caudal rami of the superior temporal sulcus. Eur J Neurosci. 2012; 36:2035–53. [PubMed: 22708629]

Smith SM. Fast robust automated brain extraction. Hum Brain Mapp. 2002; 17:143–55. [PubMed: 12391568]

Smith SM, Brady JM. SUSAN—A New Approach to Low Level Image Processing. Int J Comput Vis. 1997; 23:45–78.

Sokolov AA, Erb M, Gharabaghi A, Grodd W, Tatagiba MS, Pavlova MA. Biological motion processing: the left cerebellum communicates with the right superior temporal sulcus. Neuroimage. 2012; 59:2824–30. [PubMed: 22019860]

Sokolov AA, Erb M, Grodd W, Pavlova MA. Structural Loop Between the Cerebellum and the Superior Temporal Sulcus: Evidence from Diffusion Tensor Imaging. Cereb Cortex. 2014; 24:626–32. [PubMed: 23169930]

Sokolov AA, Gharabaghi A, Tatagiba MS, Pavlova MA. Cerebellar engagement in an action observation network. Cereb Cortex. 2010; 20:486–91. [PubMed: 19546157]

Stephan KE, Fink GR, Marshall JC. Mechanisms of hemispheric specialization: insights from analyses of connectivity. Neuropsychologia. 2007; 45:209–28. [PubMed: 16949111]

Stoodley CJ. Distinct regions of the cerebellum show gray matter decreases in autism, ADHD, and developmental dyslexia. Front Syst Neurosci. 2014; 8:92. [PubMed: 24904314]

Stoodley CJ, Schmahmann JD. Functional topography in the human cerebellum: A meta-analysis of neuroimaging studies. Neuroimage. 2009; 44:489–501. [PubMed: 18835452]

Stoodley CJ, Valera EM, Schmahmann JD. Functional topography of the cerebellum for motor and cognitive tasks: an fMRI study. Neuroimage. 2012; 59:1560–70. [PubMed: 21907811]

Stroganova TA, Nygren G, Tsetlin MM, Posikera IN, Gillberg C, Elam M, Orekhova EV. Abnormal EEG lateralization in boys with autism. Clin Neurophysiol. 2007; 118:1842–54. [PubMed: 17581774]

Szaflarski JP, Holland SK, Schmithorst VJ, Byars AW. fMRI study of language lateralization in children and adults. Hum Brain Mapp. 2006; 27:202–12. [PubMed: 16035047]

Tellmann S, Bludau S, Eickhoff S, Mohlberg H, Minnerop M, Amunts K. Cytoarchitectonic mapping of the human brain cerebellar nuclei in stereotaxic space and delineation of their co-activation patterns. Front Neuroanat. 2015; 9:54. [PubMed: 26029057]

Tiemeier H, Lenroot RK, Greenstein DK, Tran L, Pierson R, Giedd JN. Cerebellum development during childhood and adolescence: a longitudinal morphometric MRI study. Neuroimage. 2010; 49:63–70. [PubMed: 19683586]

Wechsler, D. WASI Manual. San Antonio, TX: 1999.

Weiss-Croft LJ, Baldeweg T. Maturation of language networks in children: A systematic review of 22 years of functional MRI. Neuroimage. 2015; 123:269–281. [PubMed: 26213350]

Woolrich MW. Robust group analysis using outlier inference. Neuroimage. 2008; 41:286–301. [PubMed: 18407525]

Woolrich MW, Behrens TEJ, Beckmann CF, Jenkinson M, Smith SM. Multilevel linear modelling for fMRI group analysis using Bayesian inference. Neuroimage. 2004; 21:1732–47. [PubMed: 15050594]

Woolrich MW, Ripley BD, Brady JM, Smith SM. Temporal autocorrelation in univariate linear modeling of fMRI data. Neuroimage. 2001; 14:1370–86. [PubMed: 11707093]

Worsley, KJ. Statistical analysis of activation images. In: Jezzard, P.Matthews, PM., Smith, SM., editors. Functional MRI: An introduction to methods. New York: Oxford University Press; 2001. p. 251-70.

A. Flow diagram depicting data selection process

Step 1. Initial Screening

TD Adults

Assessed for eligibility (*n* = 68)

Excluded at initial database review
• Experimenter error (*n* = 3)
• Prior exposure to paradigm (*n* = 7)
• Acquired on a different scanner (*n* = 11)

Data quality analysis (*n* = 47)

Excluded upon quality check
• Excessive motion (*n* = 2)
• Insufficient cerebellar coverage (*n* = 10)

Passed initial screen (*n* = 35) → **Step 2**

TD Children

Assessed for eligibility (*n* = 77)

Excluded at initial database review
• Experimenter error (*n* = 4)
• Acquired on a different scanner (*n* = 5)
• Missing IQ assessment (*n* = 2)

Data quality analysis (*n* = 66)

Excluded upon quality check
• Excessive motion (*n* = 14)
• Insufficient cerebellar coverage (*n* = 9)
• File corrupted (*n* = 1)

Passed initial screen (*n* = 42) → **Step 2**

Adults with ASD

Assessed for eligibility (*n* = 14)

Excluded at initial database review
• IQ < 70 (*n* = 1)

Data quality analysis (*n* = 13)

Excluded upon quality check
• Excessive motion (*n* = 2)
• Insufficient cerebellar coverage (*n* = 2)

Passed initial screen (*n* = 9) → **Step 2**

Children with ASD

Assessed for eligibility (*n* = 104)

Excluded at initial database review
• Experimenter error (*n* = 5)
• Acquired on a different scanner (*n* = 6)
• Missing IQ assessment (*n* = 1)
• Missing ADI-R (*n* = 2)
• Diagnosis inconclusive (*n* = 3)
• IQ < 70 (*n* = 5)

Data quality analysis (*n* = 86)

Excluded upon quality check
• Excessive motion (*n* = 41)
• Insufficient cerebellar coverage (*n* = 15)

Passed initial screen (*n* = 30) → **Step 2**

Step 2. Remove participants with cerebellar GM voxel loss above the 85th percentile

Passed to fMRI analysis:
N = 97
62 TD (29 Adults, 33 Children)
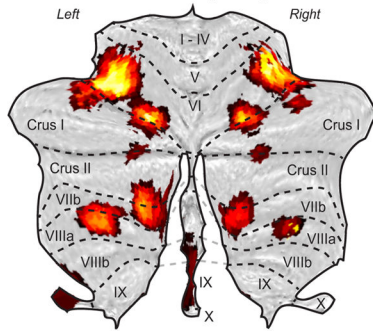35 ASD (8 Adults, 27 Children)

B. Missing voxels in final sample

TD
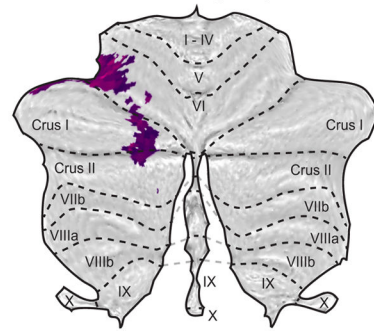-84 -72 -60 -48 -36 -24

ASD
-84 -72 -60 -48 -36 -24

Number of participants with voxel missing: 1 — 10

Figure 1.

Figure 2.

Figure 3.

Figure 4.

A. ADI-R:A and BIO > SCRAM
Controlling for age and FSIQ; n = 30
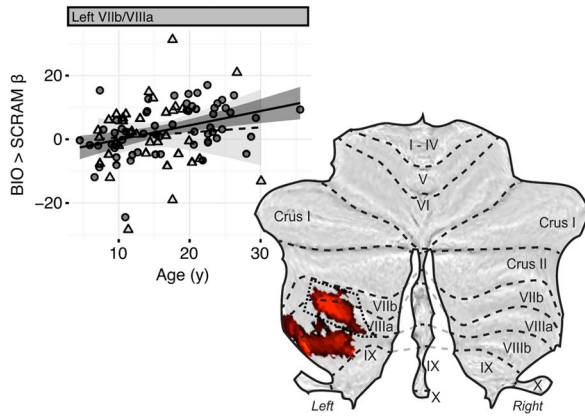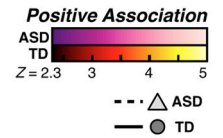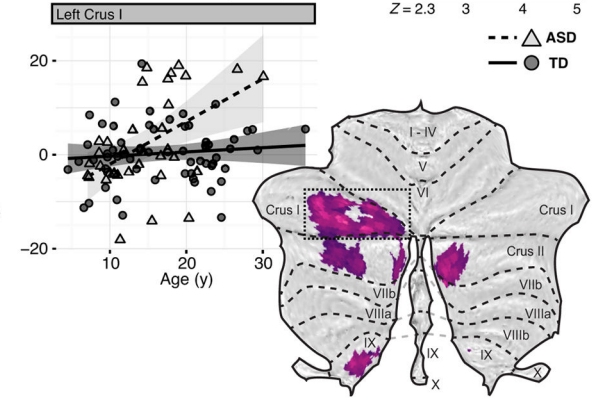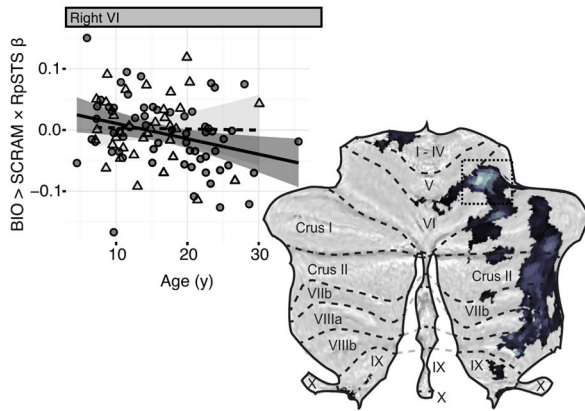
B. ADI-R:A and BIO > SCRAM × RpSTS (PPI)
Controlling for age and FSIQ; n = 30
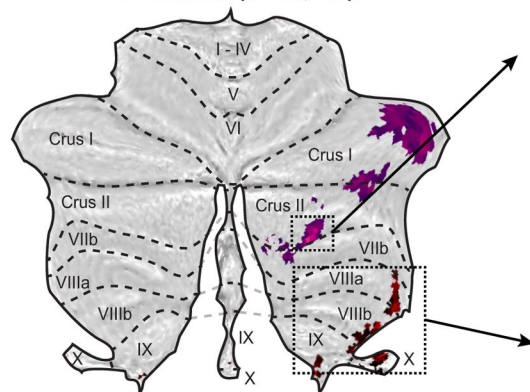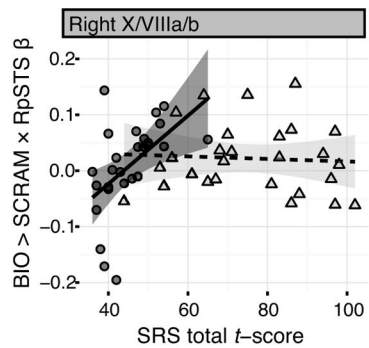
Figure 5.

A. Age and BIO > SCRAM × LpSTS (PPI)

B. ADI-R:A and BIO > SCRAM × LpSTS (PPI)
Controlling for age and FSIQ
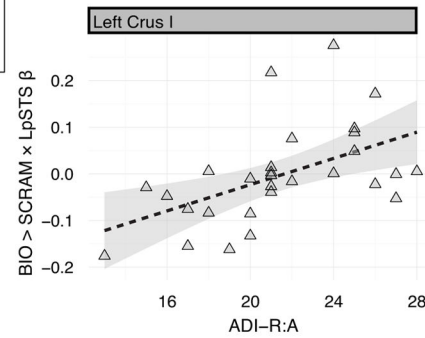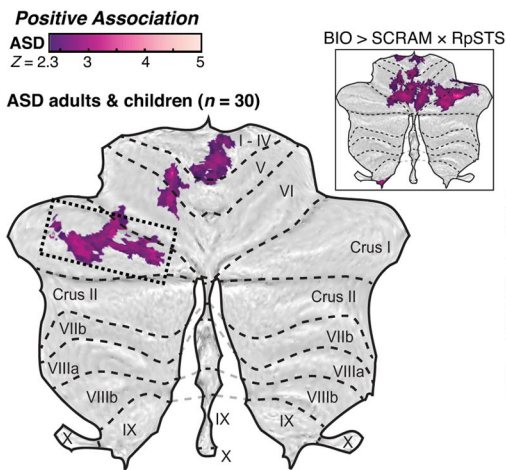
Figure 6.

Table I

Demographic, behavioral, and data quality metrics for full sample and subsamples.

A. Full Sample: Main effects and age effects within group

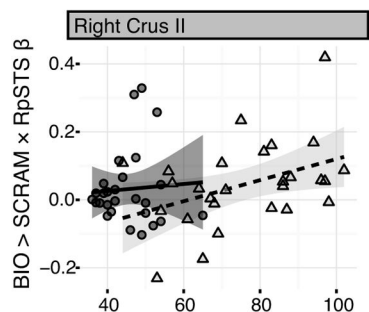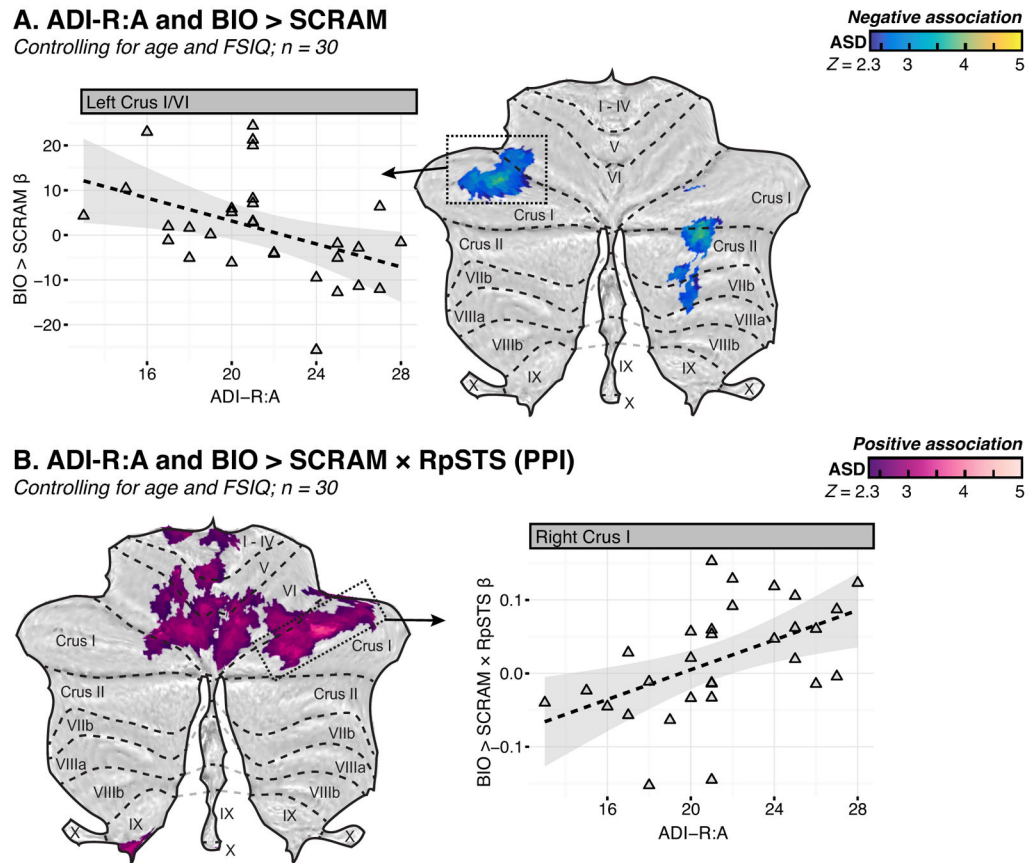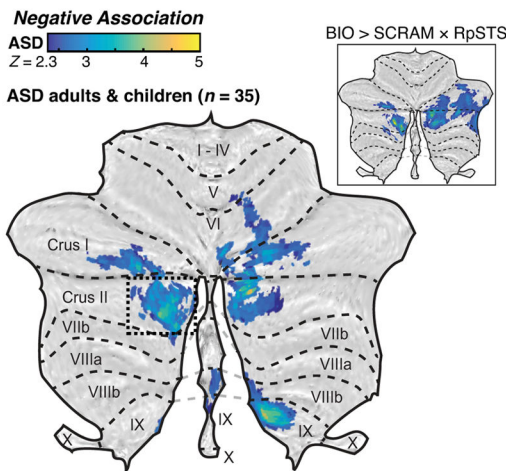|	TD n = 62 M(SD)	Range	ASD n = 35 M(SD)	Range	Diff. p
Male (n)	26		27		.891
+Age (y)	17.03(7.07)	4.50–35.58	14.49(5.40)	7.08–30.08	.051
Motion outliers (vols)	7.98(5.19)	0–23	8.03(4.96)	0–25	.967
Avg. relative RMS motion (mm)	0.08(0.03)	0.04–0.20	0.11(0.06)	0.05–0.27	.011
Max. relative RMS motion (mm)	0.51(.46)	0.11–2.25	0.88(0.66)	0.18–2.72	.004
FSIQ (not avail. for TD adults)	101.61(14.57)	78–128	97.63(18.21)	70–136	.322
ADI-R: A (avail. for 3 adults and all children)	--	--	21.37(3.79)	13–28	--
ADOS CSS	--	--	6.29(2.04)	2†–10	--

B. Matched sample (all ages): Group difference and Age x Dx interaction

	TD n = 35 M(SD)	Range	ASD n = 35 M(SD)	Range	Diff. p
Male (n)	23		27		.572
+Age (y)	14.47(6.42)	5.92–28.67	14.49(5.40)	7.08–30.08	.988
Motion outliers (vols)	9.14(5.47)	0–23	8.03(4.96)	0–25	.375
Avg. relative RMS motion (mm)	0.10(0.03)	0.04–0.20	0.11(0.06)	0.05–0.27	.335
Max. relative RMS motion (mm)	0.70(0.52)	0.17–2.25	0.88(0.66)	0.18–2.72	.210

C. Matched sample (children): SRS analyses

	TD n = 27 M(SD)	Range	ASD n = 27 M(SD)	Range	Diff. p
Male (n)	17		21		.516
+Age (y)	11.15(3.31)	5.92–17.83	12.35(3.49)	7.08–17.67	.200
Motion outliers (vols)	9.48(5.91)	0–23	8.07(5.36)	0–25	.363
Avg. relative RMS motion (mm)	0.10(0.04)	0.04–0.20	0.11(0.06)	0.05–0.27	.256

A. Full Sample: Main effects and age effects within group

	TD n = 62		ASD n = 35		Diff.
	M(SD)	Range	M(SD)	Range	p
Max. relative RMS motion (mm)	0.68(.54)	0.14–2.25	0.89(0.65)	0.18–2.72	.191
+FSIQ	101.41(14.94)	78–128	97.41(18.66)	70–136	.389
+SRS total t-score	45.25(6.84)	36–65	76.00(16.29)	44–102	<.001

D. ASD with ADI-R available

	ASD n = 30	
	M(SD)	Range
Male (n)	23	
+Age (y)	12.96(3.80)	7.08–19.00
Motion outliers (vols)	8.20(5.15)	0–25
Avg. relative RMS motion (mm)	0.11(.06)	0.05–0.27
Max. relative RMS motion (mm)	0.86(0.63)	0.18–2.72
+FSIQ	98.10(18.16)	70–136
+ADI-R: A	21.37(3.79)	13–28
ADOS CSS	6.13(2.15)	2†–10

Note. Differences on means are calculated using *t*-tests and differences on counts using chi-squared. *ADI-R: A*: Autism Diagnostic Interview-Revised Diagnostic Algorithm A: "Qualitative Abnormalities in Reciprocal Social Interaction." *ADOS CSS*: Autism Diagnostic Observation Schedule Calibrated Severity Score. *Diff.*: Difference. *FSIQ*: Full scale IQ. *Relative RMS*: Relative (volume to volume) root mean squared motion. *SRS*: Social Responsiveness Scale. +: Indicates a variable included in the group-level models run using the sample. †: This child had a low ADOS CSS but surpassed diagnostic criteria on all domains of the ADI-R and expert clinical judgment, had a well-established historical diagnosis at our clinic, and met criteria on an ADOS assessment administered later the same year.

Cluster peaks and local maxima of cerebellar regions responsive to the BIO > SCRAM contrast or to the BIO > SCRAM × RpSTS interaction in PPI analysis, controlling for age, within the full sample (sample A).

Site	Prob.	x	y	z	Z	k
BIO > SCRAM						
TD						
Left VI	77%	−32	−62	−21	5.37	774
Left VIIb	46%	−14	−72	−43	4.18	--
Left VIIIa	68%	−26	−60	−51	4.11	--
Right VI	71%	18	−68	−27	4.37	268
Right VI	49%	34	−54	−21	4.94	252
Right Crus I	66%	42	−64	−23	3.32	--
Vermis IX	89%	2	−58	−37	2.92	92
Right VIIIa	90%	28	−56	−55	7.97	49
Left Dentate	31%	−18	−52	−35	2.82	32
Left X	69%	−18	−40	−43	2.81	19
ASD						
Left VI	57%	−34	−44	−25	3.12	125
Left Crus I	71%	−20	−68	−35	2.99	92
Left VI	95%	−18	−68	−31	2.98	--
Left Crus II	78%	−18	−74	−37	2.73	--
BIO > SCRAM × RpSTS						
TD						
Left Crus I	25%	−20	−70	−35	3.13	99
Left Crus II	83%	−14	−82	−39	2.98	--
Left VI	97%	−28	−56	−23	3.07	26
Left VIIIb	48%	−28	−38	−51	3.00	26
Right X	86%	24	−34	−43	2.99	19
Right VIIIb	68%	28	−42	−47	2.65	--
ASD						

Site	Prob.	x	y	z	Z	k
Left Crus II	67%	−40	−78	−43	3.81	419
Left Crus II	100%	−14	−90	−37	3.78	--
Right Crus I	100%	28	−86	−27	4.07	319
Right Crus II	50%	26	−84	−35	3.31	--
Right VIIIb	58%	8	−64	−55	4.38	240
Right IX	96%	2	−54	−51	3.82	--

Note. Coordinates are reported in MNI space. Probability (Prob.) indicates the degree of certainty with which the cluster coordinates can be assigned to the indicated lobule according to the probabilistic SUIT atlas. *Z*: *Z*-statistic. *k*: Cluster voxel extent.

Table III

Cluster peaks and local maxima of cerebellar regions where age was associated with BIO > SCRAM response or with the BIO > SCRAM × RpSTS/ LpSTS interaction in PPI analysis, within the full sample (sample A, TD $n = 62$, ASD $n = 35$).

Site	Prob.	x	y	z	Z	k
Age & BIO > SCRAM: Positive associations						
TD						
Left VIIIb	30%	−28	−36	−51	3.89	272
Left VIIIb	85%	−14	−52	−55	3.76	--
Left VIIIa	59%	−30	−56	−51	3.58	--
ASD						
Left Crus I	99%	−28	−68	−33	3.78	424
Left Dentate	48%	−10	−68	−33	3.13	--
Right Crus II	50%	8	−76	−43	3.43	66
Left IX	63%	−8	−46	−51	3.27	66
Age & BIO > SCRAM × RpSTS: Negative associations						
TD						
Right VIIb	73%	38	−54	−53	4.51	459
Right VIIa	51%	38	−46	−55	4.4	--
Right VIIIb	96%	20	−46	−55	4.16	--
Right VI	54%	24	−50	−29	4.73	445
Right Crus I	100%	32	−78	−25	2.9	--
Left I-IV	66%	−18	−34	−21	3.09	338
ASD						
Right Crus I	63%	14	−82	−31	3.92	885
Right Crus II	97%	16	−84	−41	3.64	--
Left Crus II	99%	−22	−84	−43	4.96	514
Left Crus I	100%	−36	−82	−33	3.63	--
Age & BIO > SCRAM × LpSTS: Negative associations						
ASD						
Left Crus II	86%	−20	−90	−35	4.73	775

Site	Prob.	x	y	z	Z	k
Right Crus II	95%	14	−86	−31	4.33	
Right Crus II	66%	4	−84	−35	3.83	
Left Crus II	79%	−14	−82	−41	3.68	
Right IX	100%	4	−56	−51	4.24	183
Vermis VIIIb	67%	4	−64	−47	2.97	

Note. Coordinates are reported in MNI space. Probability (Prob.) indicates the degree of certainty with which the coordinates can be assigned to the indicated lobule according to the SUIT atlas. *Z*: *Z*-statistic. *k*: cluster voxel extent.

Table IV

Cluster peaks and local maxima of cerebellar regions where SRS total t-score predicted BIO > SCRAM response or the BIO > SCRAM × RpSTS interaction in PPI analysis, controlling for age and FSIQ, within a matched sample of TD children and children with ASD (sample C).

Site	Prob.	x	y	z	Z	k
SRS & BIO > SCRAM: Negative Associations						
TD						
n.s.						
ASD						
Right Dentate	40%	20	−54	−33	2.84	33
SRS & BIO > SCRAM × RpSTS: Positive Associations						
TD						
Right X	68%	24	−34	−45	3.23	134
Vermis X	50%	4	−46	−39	3.08	--
Right VIIIa	32%	34	−38	−47	3.06	--
ASD						
Right Crus I	100%	46	−54	−29	3.24	89
Right Crus II	58%	26	−76	−49	3.62	61
Right VIIb	73%	18	−76	−51	2.94	--
Right Crus I	78%	44	−78	−39	3.38	57

Note. Coordinates are reported in MNI space. Probability (Prob.) indicates the degree of certainty with which the cluster coordinates can be assigned to the indicated lobule according to the probabilistic SUIT atlas. Z: Z-statistic. k: Cluster voxel extent.

Table V

Cluster peaks and local maxima of cerebellar regions where ADI-R diagnostic algorithm A, "Qualitative abnormalities in reciprocal social interaction," was associated with BIO > SCRAM response or with the BIO > SCRAM × RpSTS/LpSTS interaction in PPI analysis, controlling for age and FSIQ, among individuals with ASD for whom the ADI-R was available (sample D).

Site	Prob.	x	y	z	Z	k
ADI-R:A & BIO > SCRAM: Negative associations						
Left Crus I	100%	−38	−64	−27	3.88	215
Left VI	81%	−28	−54	−29	3.25	--
Right Crus II	55%	26	−70	−39	3.84	173
Right VIIb	29%	26	−64	−45	2.99	--
ADI-R:A & BIO > SCRAM × RpSTS: Positive associations						
Right Crus I	100%	38	−66	−27	3.89	1356
Left VI	88%	−24	−74	−21	3.57	--
Left V	88%	−16	−50	−13	3.53	--
Right VI	45%	12	−70	−13	3.46	--
ADI-R:A & BIO > SCRAM × LpSTS: Positive associations						
Left V	88%	−16	−50	−13	3.52	174
Left VI	87%	−18	−60	−15	3.14	
Right I-IV	100%	4	−48	−9	3.06	
Left Crus I	70%	−26	−80	−23	3.43	155
Left Crus I	100%	−44	−64	−31	3.26	
Left VI	38%	−26	−76	−21	2.96	

Note. Coordinates are reported in MNI space. Probability (Prob.) indicates the degree of certainty with which the cluster coordinates can be assigned to the indicated lobule according to the probabilistic SUIT atlas. *Z*: *Z*-statistic. *k*: Cluster voxel extent.